Photodiagnosis and Photodynamic Therapy 31 (2020) 101913

Contents lists available at ScienceDirect

Photodiagnosis and Photodynamic Therapy

journal homepage: www.elsevier.com/locate/pdpdt

Vaterite submicron particles designed for photodynamic therapy in cells

Eliane F. Souza, Jéssica A.R. Ambrósio, Bruna C.S. Pinto, Milton Beltrame, Kumiko K. Sakane, Juliana G. Pinto, Juliana Ferreira-Strixino, Erika P. Gonçalves, Andreza R. Simioni*

Research and Development Institute – IPD. Vale do Paraíba University, UNIVAP. Av. Shishima Hifumi, 2911, CEP: 12244-000, São José dos Campos, SP, Brazil

ARTICLE INFO

Keywords:
Photosensitizer
Vaterite submicron particles
Calcium carbonate
Photodynamic therapy

ABSTRACT

Background: Calcium carbonate ($CaCO_3$) is one of the most abundant materials in the world. It has several different crystalline phases as present in the minerals: calcite, aragonite and vaterite, which are anhydrous crystalline polymorphs. Regarding the preparation of these microparticles, the most important aspect is the control of the polymorphism, particle size and material morphology. This study aimed to develop porous microparticles of calcium carbonate in the vaterite phase for the encapsulation of chloro-aluminum phthalocyanine (ClAlPc) as a photosensitizer (PS) for application in Photodynamic Therapy (TFD).

Methods: In this study, spherical vaterite composed of microparticles are synthesized by precipitation route assisted by polycarboxylate superplasticizer (PSS). The calcium carbonate was prepared by reacting a mixed solution of Na_2CO_3 with a $CaCl_2$ solution at an ambient temperature, 25 °C, in the presence of polycarboxylate superplasticizer as a stabilizer. The photosensitizer was incorporated by adsorption technique in the $CaCO_3$ microparticles. The $CaCO_3$ microparticles were studied by scanning electron microscopy, steady-state, and their biological activity was evaluated using *in vitro* cancer cell lines by trypan blue exclusion method. The intracellular localization of ClAlPc was examined by confocal microscopy.

Results: The $CaCO_3$ microparticles obtained are uniform and homogeneously sized, non-aggregated, and highly porous microparticles. The calcium carbonate microparticles show an average size of 3 μm average pore size of about 30–40 nm. The phthalocyanine derivative loaded-microparticles maintained their photophysical behavior after encapsulation. The captured carriers have provided dye localization inside cells. The *in vitro* experiments with ClAlPc-loaded $CaCO_3$ microparticles showed that the system is not cytotoxic in darkness, but exhibits a substantial phototoxicity at 3 $\mu mol.L^{-1}$ of photosensitizer concentration and 10 $J.cm^{-2}$ of light. These conditions are sufficient to kill about 80 % of the cells.

Conclusions: All the performed physical–chemical, photophysical, and photobiological measurements indicated that the phthalocyanine-loaded CaCO3 microparticles are a promising drug delivery system for photodynamic therapy and photoprocesses.

1. Introduction

The systemic or topical administration of a photosensitizer (PS) should result in the specific accumulation and retentionof this drug in neoplastic areas. . Light excitation of the PS then causes the production of cytotoxic reactive oxygen species (ROS), such as singlet molecular oxygen ($^1O_2$), and consequently to cell death [1–3].

The chemical structures of PSs are diverse, and, accordingly, the biological behavior of tetrapyrrole-based photosensitizer can be quite different one to the other [4], but in a PDT process, PSs are critical to the successful eradiation of malignant cells [5]. The first-generation PS refers to Hematoporphyrin (Hp) and Hematoporphyrin derivative (HpD) [6]. Second generation PSs were developed aiming to solve deficiencies and limitations presented by the first-generation drugs as weak absorbance in the red region of the spectrum, poor selectivity in terms of target tissue/healthy tissue ratios and a low molar extinction coefficient that requires use high doses of PS and light for adequate tumor eradication [7]. The second-generation photosensitizers include phthalocyanines, naphthalocyanines, chlorines and bacteriochlorines [8,9]. These compounds shown high absorption properties in the therapeutic window, low toxic side effects and exhibited higher intracellular $^1O_2$ generation, the main responsible of cancer cell death [10,11]. However, most of these agents are very hydrophobic and show low tumor selectivity [12]. The most promising strategy to improve PS selectivity is to develop drug delivery systems that can incorporate lipophilic photosensitizers and are highly selective for tumour cells

* Corresponding author.
E-mail address: simioni@univap.br (A.R. Simioni).

https://doi.org/10.1016/j.pdpdt.2020.101913
Received 31 May 2020; Received in revised form 26 June 2020; Accepted 2 July 2020
Available online 06 July 2020

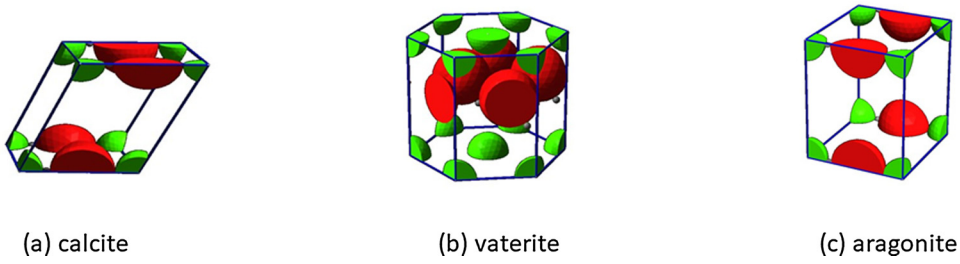

Fig. 1. Unit cells of the polymorphic phases of $CaCO_3$: a) calcite, b) vaterite, c) aragonite.

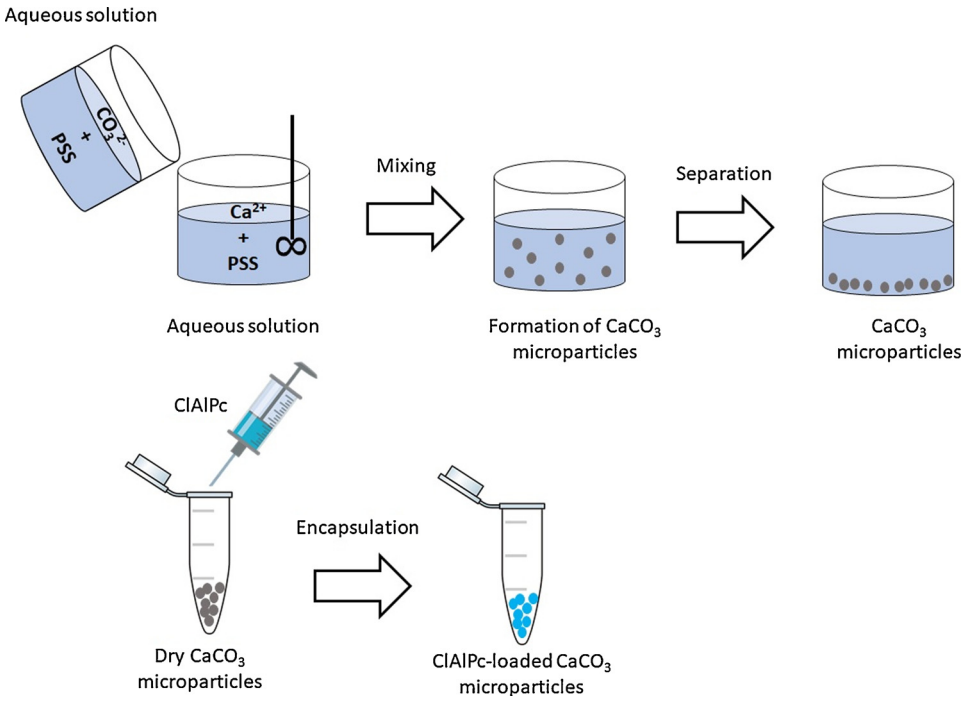

Fig. 2. Chemical precipitation procedure for preparation of $CaCO_3$ microparticles.

[13,14].

Recently, porous inorganic materials are emerging as a new category of delivery system for bioactive compounds due to some characteristics such as biological stability and controlled release property [15].

Calcium carbonate ($CaCO_3$) is one of the most important industrial and biological materials due to its abundance in nature and its wide applications in pharmaceutical and medication areas [16]. $CaCO_3$ has three anhydrous crystalline polymorphs: vaterite, aragonite, and calcite [17] (Fig. 1). The morphological forms of calcium carbonate are related to the synthesis conditions, such as the concentration of reactants, temperature, and nature of additives [18–20]. The unit cells of the polymorphic phases of $CaCO_3$ were

constructed using the app crystalwlak (https://crystalwalk.herokuapp.com). Recent researchers found that vaterite is composed of a major phase of hexagonal symmetry filled with amorphous nanodomains [21].

Vaterite particles can be loaded with a variety of active substances, which leads to distribution both on the surface and inside the particles due to their porous structure [22]. Vaterite matrix are generally biocompatible, with low toxicity, and a high loading volume [23]. All these characteristics make them attractive as a delivery system for photosensitizer for treatment of cancer by protocols PDT application.

Thereby, in this work we focused on the synthesis, photochemical characterization and photobiological assays for sustained drug release of adsorption in porous vaterite $CaCO_3$ submicron particles. This is an innovative study of a drug delivery system with a chloroaluminum phthalocyanine (ClAlPc)-loaded porous vaterite CaCO3 microparticles using macrophages cell as biological model for PDT protocols application.

2. Materials and methods

2.1. Materials

Sodium poly(styrene sulfonate) (PSS, Mw ~ 70 KDa) and the photosensitizer chloroaluminum phthalocyanine (ClAlPc) were purchased from Sigma-Aldrich. The calcium chloride ($CaCl_2$), sodium carbonate (Na_2CO_3) and ethylenediaminetetracetic acid (EDTA) were purchased from Neon (Brazil). All other chemicals are of analytical grade and were used promptly.

2.2. Synthesis of vaterite $CaCO_3$ submicron particles

Vaterite $CaCO_3$ submicron particles were prepared by chemical precipitation procedure by rapid mixing of equal volume of $CaCl_2$ and Na_2CO_3 aqueous solutions as describe by Saraya et al. [24] with modifications. Typically, 0.2 $mol.L^{-1}$ Na_2CO_3 (pH = 11.2) reacted with 0.5 $mol.L^{-1}$ $CaCl_2$ (pH = 6.7) solutions in the presence of 2% polycarboxylate-type superplasticizer at room temperature and was sonicated during 11 min using mechanical stirring process at high-speed from an ultra-turrax setup to optimize the preparation of the vaterite

$CaCO_3$ microparticles. After vigorous agitation, the precipitate was filtered off, thoroughly washed with pure water, and dried in air. The simple procedure results in highly homogeneous spherical porous $CaCO_3$ microparticles with an average diameter of 3 μm.

For loading the ClAlPc, 0.5 g of dried $CaCO_3$ microparticles were soaked in 5 mL ClAlPc Afterward, the suspension was brought to equilibrium under gentle stirring for 24 h. Subsequently, the ClAlPc-loaded $CaCO_3$ microparticles were collected by centrifugation, washed with ethanol to remove the adsorbed ClAlPc on the external surface, and dried in a vacuum oven at 50 ∘C to completely evaporate the solvent from the impregnated materials (Fig. 2).

2.3. Morphology characterization

To study the morphology and microstructure, dried particles were sputtered with gold and imaged with a scanning electron microscope (SEM) using EVO-MA10 (Zeiss) with tungsten filament at the acceleration voltage of 20 kV.

2.4. Brunauera–Emmeta–Teller (BET) method

The specific surface area of the calcium carbonate particles and size distribution of the particle pores were evaluated using a NOVA 220e analyzer (Quantachrome, United States) using the physical gas adsorption method with subsequent calculation of the specified parameters by means of a special software tool integrated into the device. A sample of the investigated substance was preliminarily degassed in vacuum at a temperature of 35 °C for 5 days, and then the adsorption isotherm was obtained. Nitrogen was used as an absorbate. The Brunauera–Emmeta–Teller (BET) method was applied to calculate the specific surface areas. The size distribution of pores was defined using the Barrett–Joyner–Halenda (BJH) method.

2.5. X-ray diffraction (XRD)

The X-ray diffraction (XRD) studies were performed to study the crystalline phases of synthesized calcium carbonate products. The XRD spectra were recorded on (M/S. Shimadzu Instruments, Japan) diffractometer XRD 6000 with Ni filtered Cu Kα as a radiation source at 2θ scan speed of 2∘ min^{-1}, k =1.54439 Å.

2.6. Fourier transform infrared (FT-IR) spectroscopy

Fourier transform Infrared (FT-IR) spectra were measured using a Spectrum Spotlight 400 FT-IR spectrometer (Perkin Elmer) with the KBr pellet method. The sample was good ground and thoroughly mixed to homogenize them. The homogenized sample was mixed with dry KBr in 1:100 mass ratios and pellet were pressed at 5 Tons. The spectra of the sample pellets were recorded by using pure KBr pellet as the blank.

2.7. Steady state measurements

Absorption measurements were carried out for the sample in ClAlPc, with a Cary 50 BIOVarian Inc. Scientific Instruments that was background corrected using matched quartz cuvettes with scanning over the wavelength range from 500 to 800 nm. To establish linearity of the proposed methods a calibration curve was constructed at eight concentrations levels within the range of 0.50–3.00 μmol.L^{-1} for the spectrophotometric method. In the spectrophotometric analyses the Beer's law was obeyed. Least square regression analysis was done for the data. One-way analysis of variance (ANOVA) and a Lack-of-fit test ($p = 0.05$) were used to determine whether the linear model adequately explains obtained data.

2.8. Loading capacity (%LC)

To estimate the mass of ClAlPc loaded into $CaCO_3$ containers, their weighed portion was dissolved in aqueous solution of ethylenediaminetetracetic acid (EDTA, 0.2 M). As a measure of the amount of ClAlPc in solution, absorbance intensity was recorded at 674 nm, which corresponds to the maximum absorption wavelength (λ_{max}) of ClAlPc.

The loading capacity (%LC) of containers was estimated according to equation:

$$\%LC = \frac{m(ClAlPc\ loaded)}{m\ (particles)} x\,100\%$$

where: *m(ClAlPc loaded)* is the weight of ClAlPc incorporated into $CaCO_3$ particles, (*mparticles)* – the weight of $CaCO_3$ particles.

Analyses were performed in triplicate and the mean results (± SD) are reported. All results obtained were compared using a Tukey post-test, and statistical significance was considered at $p < 0.05$.

2.9. In vitro experiments

2.9.1. Cell cultures

The Murine RAW 264.7 cell line was acquired at the Rio de Janeiro Cell Bank (BCRJ) - Brazil, where they were tested and found to be free from contamination and maintained in DMEM medium (Dulbecco's Modified Eagle Medium) purchased from Sigma Aldrich, supplemented with 10 % Bovine Fetal Serum, 1% Penicillin / Streptomycin solution (LGC Biotechnology), packed in a 37 °C incubator with 5% of CO2.

2.9.2. Dark cytotoxicity assay

All tests were performed in triplicate in 96-well plates, and the cell concentration was 5×10^6 cells per well. To the tests with ClAlPc incorporated into $CaCO_3$ particles, it was applied with the concentrations of 0,6 μmol.L^{-1}, 3,0 μmol.L^{-1} and incubated for 1 h in a growing chamber at 37 °C. After incubation time, the medium with microparticles was withdrawn and it was added to 200 μl of PBS in each well. The dark groups were kept in the dark, and irradiated groups were submitted to light exposure in the biotable. After irradiation, the PBS was withdrawn from all groups, substituted for a fresh medium, and maintained at 37 °C for 18 h, before the trypan blue assays.

2.9.3. Photocytotoxicity assay

The LED device (Biopdi/IRRAD-LED 660 nm) used in the PDT experiments is composed by 54 LEDs, and each LED presents a potency of 70 mW, emitting in 660 ± 5 nm and covering a area of 150 cm^2. The intensity used was 25 mW.cm^{-2}, and the exposure time was 6 min and 40 s, totalizing the energy density of 5 and 10 J.cm^{-2}. The intensity was found following the formula: (54 × 70) /A═I, and the fluency was found following the formula: I (W.cm^{-2}) × t (s) = F (J. cm^{-2}). The dark groups were kept in the dark, and irradiated groups were submitted to light exposure in the biotable.

2.10. Cellular viability analysis through the trypan blue exclusion method

For the trypan blue exclusion test, 18 h after the treatments, as described in the incubation protocol above, the medium was removed and 50 μl of trypan blue (2%) (Sigma®) was added. After 5 min of incubation, 150 μl of PBS was added and they were made with photos of five random sites. The alive and dead cells were counted using the ImageJ® cell counter.

2.11. Intracellular localization of ClAlPc

To determine PS internalization the cells were incubated with 0,6 μmol.L^{-1} and 3,0 μmol.L^{-1} ClAlPc incorporated into $CaCO_3$ particles for one hour in an oven at 37 °C. After this period, the PS was removed, the wells washed with PBS and added with 100 μl of 4% paraformaldehyde.

After fixation, labeling with DAPI (4′, 6-diamidino-2-phenylindole, dihydrochloride) (Thermofisher - ProLong ™ Diamond Antifade Mountant with DAPI) was performed for DNA labeling. All processing was performed in the dark, and the slides examined under a confocal microscope LSM 700 Zeiss.

2.12. Statistical analysis

All tests were performed in triplicate, and all data were submitted to ANOVA followed by Turkey test. Microsoft Excel was used to generate the charts. All data are expressed as the mean ± standard deviation (SD) of three independent experiments. A probability p-value < 0.05 was considered significant in this study.

3. Results

The $CaCO_3$ microparticles were prepared by chemical precipitation procedure by the reaction of calcium ions from aqueous solution of calcium chloride, and carbonate ions from aqueous solution of sodium carbonate. Reaction between two phases leads to formation of microparticles which were separated through centrifugation.

Fig. 3 shows that $CaCO_3$ were synthesized in the presence and absence of PSS.

The results exhibit that in the absence of the PSS system, $CaCO_3$ only formed common very crystalline, cubic crystal calcite crystal structure (Fig. 3a). Fig. 3(b, c) indicate the morphology of $CaCO_3$ crystal prepared by adding PSS. On the other hand, the PSS as superplasticizer influences crystal growth and, the spherical morphology of final vaterite calcium carbonate are formed.

Porosity is an important feature of $CaCO_3$ microparticles. We applied the Brunauer–Emmett–Teller (BET) method of nitrogen adsorption/desorption to determine the surface area of $CaCO_3$ microparticles (mean diameter 3 μm) and an effective pore size distribution. The specific surface area of microcontainers estimated by the BET method is 22 m^2/g. The average pore size of the sample is 37.2 ± 0.2 nm (Fig. 4).

A spherical shape of the particles indicates the vaterite phase of $CaCO_3$, that was proved out by the XRD data presented in Fig. 5.

The XRD pattern of pure $CaCO_3$ microparticles exhibits the characteristic reflection for vaterite owning to the peaks corresponding to (102), (110) and (112) planes. The peaks, which are typical for calcite phase of $CaCO_3$, were not observed on the XRD pattern.

The IR spectra of the $CaCO_3$ microparticles, free ClAlPc and ClAlPc-loaded $CaCO_3$ microparticles are shown in Fig. 6.

The IR spectrum of the ClAlPc-loaded $CaCO_3$ microparticles reflects the characteristic absorption bands of ClAlPc and calcium carbonate without obvious new bands, which indicates that ClAlPc adsorption in $CaCO_3$ is of physical.

Fig. 7 shows the typical absorption spectra of free ClAlPc and ClAlPc-loaded $CaCO_3$ microparticles.

All the spectra are characterized by strong Q-band in the visible region by the appearance of characteristic peaks for ClAlPc at 674 nm.

The compound showed monomeric behavior in the concentration

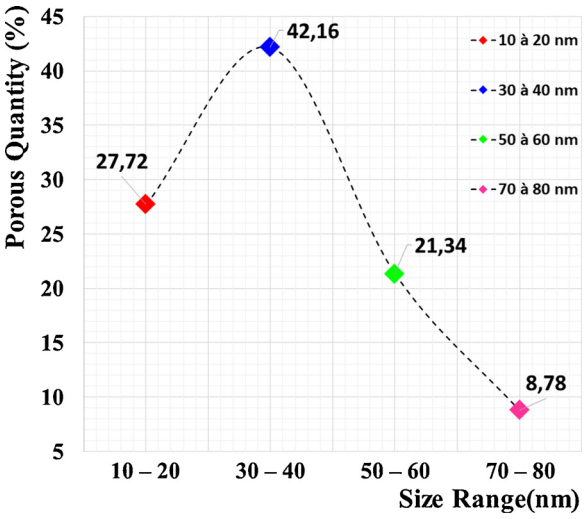

Fig. 4. Size distribution of pores in the calcium carbonate particles.

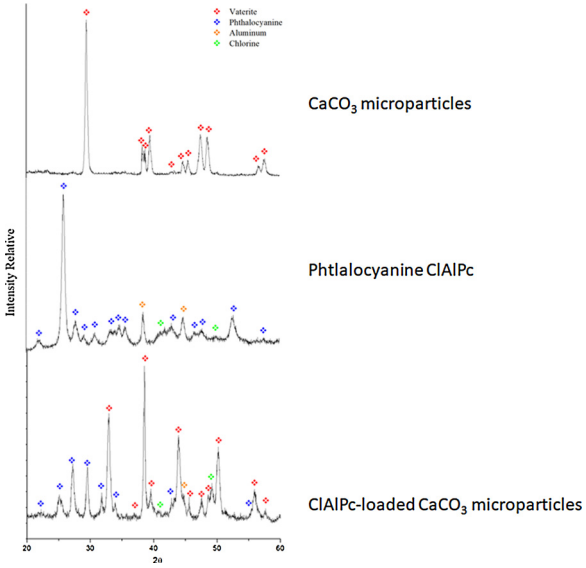

Fig. 5. XRD data of pure and ClAlPc-loaded $CaCO_3$ particles.

range studied (from 0.5 μmol.L^{-1} to 3.0 μmol.L^{-1}), as it is possible to see in ethanol in Fig. 8a.

Least square regression for spectrophotometric method showed excellent correlation coefficient (r = 0,99185) and the straight-line equation was: absorbance = 0,27719. [ClAlPc concentration, μmol.L^{-1}] + 0,08629 (Fig. 8b). Satisfactory loading efficiency was obtained (83,8 % ± 1,1).

The results of trypan blue exclusion test have shown significant

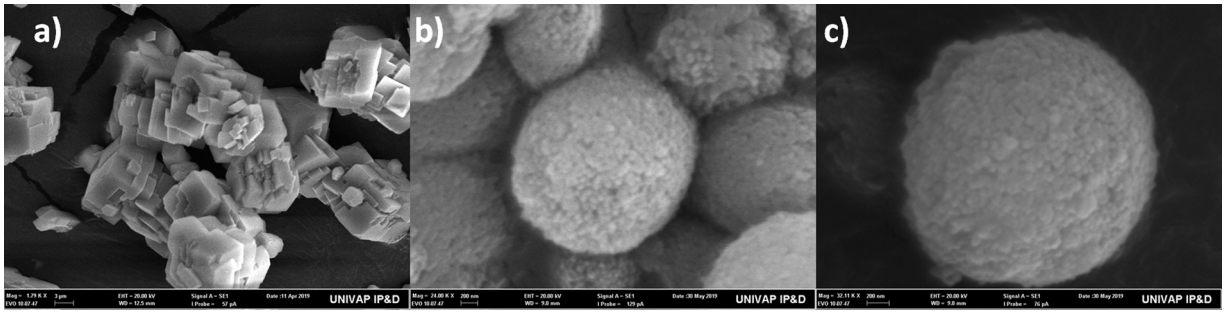

Fig. 3. Scanning electron microscopy images of $CaCO_3$ particles formed in absence (a) and in the presence of PSS (b, c).

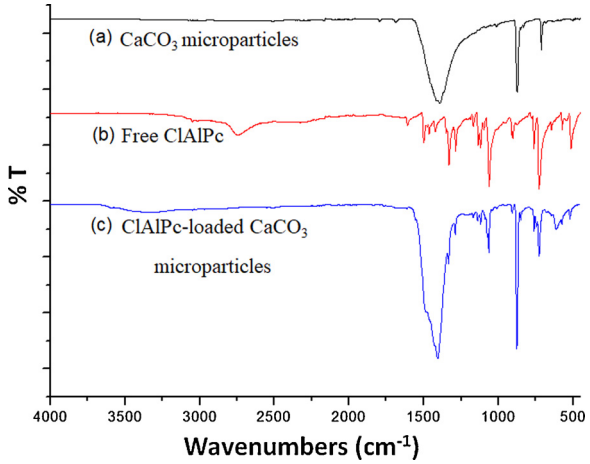

Fig. 6. IR spectra of (a) $CaCO_3$ microparticle, (b) ClAlPc microcrystal and (c) ClAlPc-loaded $CaCO_3$ microparticle.

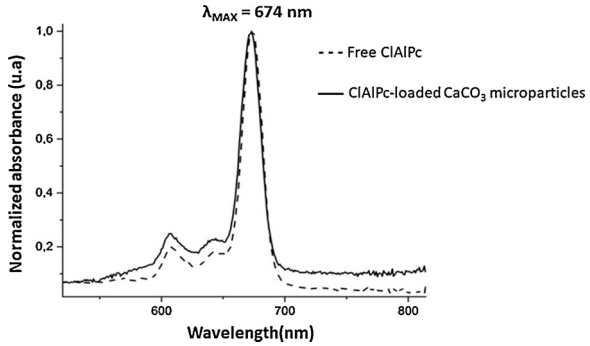

Fig. 7. Normalized optical absorption spectra of free ClAlPc (- -) and ClAlPc-loaded $CaCO_3$ microparticle (-).

reduction ($p < 0.05$) in the cell viability for all groups treated with PDT, in all concentrations tested (Fig. 9).

There was no significant difference observed between the control group and the irradiated group without the PS. No differences were observed between these groups and the group with free ClAlPc without irradiation in the highest concentration, showing low cytotoxicity of the PS in the absence of light, indicating that in the first case, the interaction of light with the cell does not induce cell death or proliferation, and in the

second case, the photosensitizer in the absence of light was non-cytotoxic to this cell line, in the parameters used in this study.

It is possible to observe a significant reduction in viability, in the groups treated with the highest concentration, of ClAlPc-loaded $CaCO_3$ 3 μmol.L^{-1}, with approximately 80 % reduction in the group treated with 10 J.cm-^{2}. These data suggest a result dependent on the concentration of phthalocyanine and the dose of light used. With a dose of 5 J.cm-^{2}, a reduction in viability was observed after PDT with 0.6 μmol.L^{-1}, however the result was not significant.

After 1 h of incubation, it was observed that the ClAlPc-loaded $CaCO_3$ was inside the cell, located in the cytoplasm, and a specific accumulation was observed in the nucleus (Fig. 10).

4. Discussion

Biomimetic precipitation reaction methods include the spontaneous precipitation reaction and the slow carbonation reaction. The spontaneous precipitation reaction is the main and easiest way to prepare $CaCO_3$ particles as it basically involves the mixing of CO_3^{2-} and Ca^{2+} solutions containing the additives [25]. The inclusion of additives in the reaction mixture, are shown to exert a strong effect on the morphology of the formed $CaCO_3$ microparticles [26–28]. The presence of PSS molecules in the crystallizing solution promoted a significant change in the morphology of the precipitated calcium carbonate inorganic particles [29]. The SEM image of $CaCO_3$ obtained in the absence of PSS revealed the formation of large crystals with rhombohedral morphology, as expected under these experimental conditions [30]. On the other hand, smaller particles with spherical morphology were obtained when precipitation occurred in the presence of PSS. Vaterite is the main shape in all the samples produced in the presence of PSS. The $CaCO_3$ microparticles obtained by this simple route are uniform and homogeneously sized, non-aggregated, highly porous spheres with a narrow size distribution of 3 μm.

The Brunauera–Emmeta–Teller (BET) method revealed that the obtained vaterite $CaCO_3$ microparticles were porous. Vaterite synthesized had the BET specific surface area of around 22 m^2. g^{-1}. Beuvier et al. synthesized porous crystalline calcium carbonate microspheres composed of vaterite with the high specific surface area of 16 m^2. g^{-1} deduced from nitrogen absorption/desorption isotherms, which confers an important porosity to the microspheres [31]. The average pore size of the sample is 37.2 ± 0.2 nm A spherical shape of the particles indicates the vaterite phase of $CaCO_3$, that was proved out by the XRD data presented in Fig. 6. The XDR analysis of ClAlPc-loaded vaterita microparticles shows that the photosensitizer molecules are adsorbed on the pores of the microparticles, since the displacement of the peaks of vaterita was observed, which showed approximately 0.02° increase in diffraction angle.

For photosensitizer encapsulation experiments, we used 3 μm particles which provided increased surface area for adsorption/porous diffusion of larger amounts of photosensitizer [32]. ClAlPc-loaded $CaCO_3$ particles were prepared by physical adsorption technique where the active substance should be adsorbed from the solution onto preformed particles, this method allows one to encapsulate five times

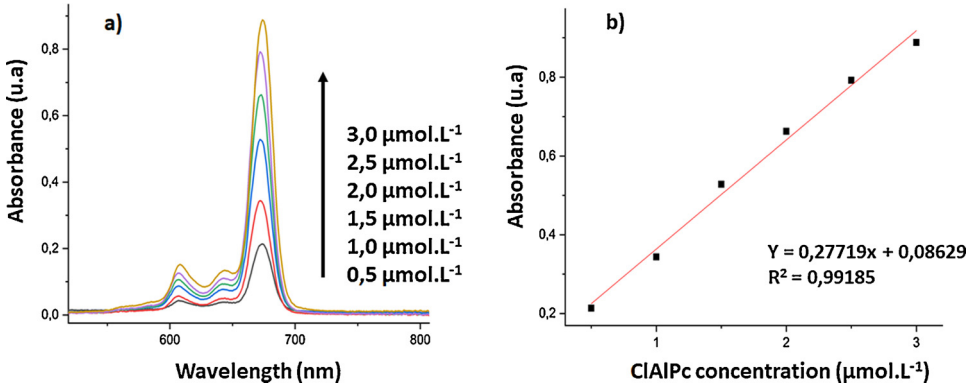

Fig. 8. (a): Absorption spectra of ClAlPc at different concentrations (0.5 - 3.0 μmol.L^{-1}); (b): plot of ClAlPc concentration *vs.* absorbance.

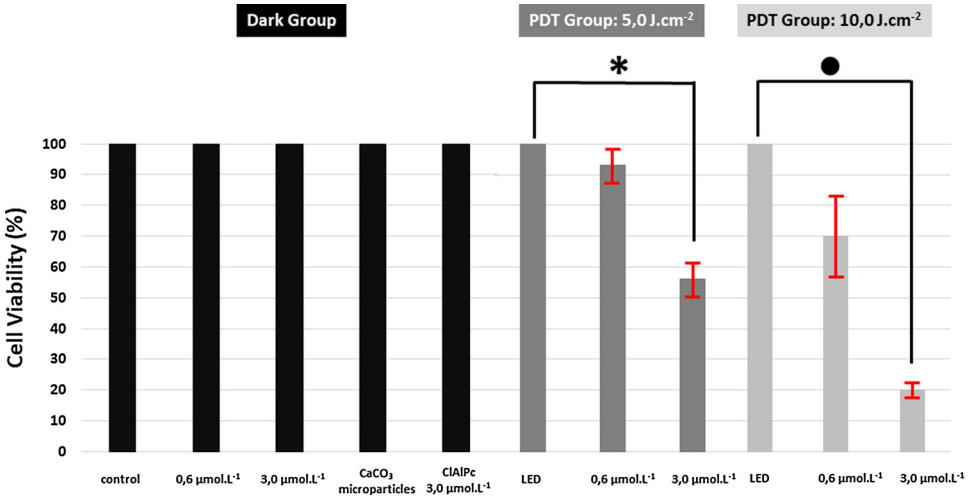

Fig. 9. Evaluation of cell viability with the trypan blue exclusion method; *($p < 0.05$).

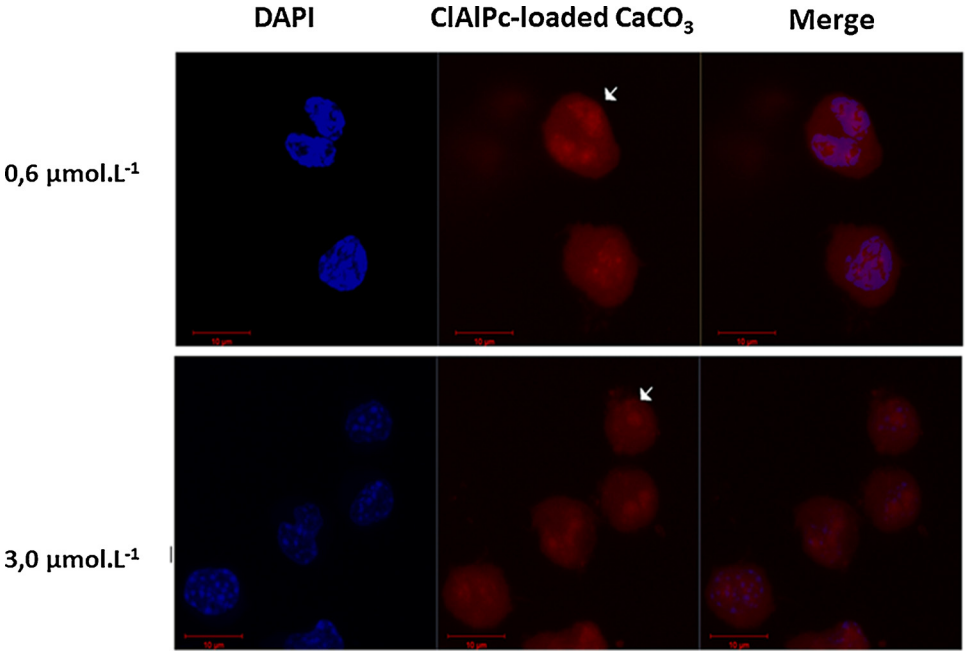

Fig. 10. Cellular internalization of ClAlPc-loaded $CaCO_3$ particles visualized by laser scanning confocal microscope.

higher amounts of biologically active substance [33].

FT-IR spectrum, given in Fig. 6a, clearly shows major bands centred at 1088 and 1413 cm^{-1} wavenumbers. These IR-bands correspond to those of vaterite polymorph of calcium carbonate [34]. The IR spectrum of the ClAlPc-loaded $CaCO_3$ microparticles reflects adsorption in $CaCO_3$ is of physical, since there were without obvious new bands in the spectrum. Wang et al. describe this behavior in the adsorption of ibuprofen into the porous $CaCO_3$ microparticles [35].

UV/Vis spectra of the ClAlPc-loaded $CaCO_3$ microparticles showed that the microparticles displayed similar absorption features to free ClAlPc with Q-bands at 674 nm, which corresponds to the maximum absorption wavelength (λ_{max}) of ClAlPc. No shift of the maximum absorption at Q-band can be observed, suggesting that the photosensitizer was mainly in a monomeric form without aggregation inside the microparticles. This indicates that the photophysical properties of ClAlPc molecules in the microparticles were well retained [36].

In trypan blue exclusion test, the dye penetrates into membranes of dead cells since dead cells have damaged membranes, whereas the dye is excluded from live cells with intact cell membrane so that dead cells are seen as blue under light microscope [37]. It It is possible to observe a significant reduction in viability, in the groups treated with the highest concentration, of 3 µmol.L^{-1}, reaching approximately 80 % reduction in the group treated with 10 J.cm-^{2}. These data suggest a result dependent on the concentration of phthalocyanine and the dose of light used. With a dose of 5 J.cm-^{2}, a reduction in viability was observed after PDT with 0.6 µmol.L^{-1}, however the result was not significant. It is important to note that in the control groups, kept in the dark, there was no reduction in viability, demonstrating that phthalocyanine is not cytotoxic to macrophages, under these conditions tested.

Svenskaya et al. (2016) encapsulated the Photosen photosensitizer in microparticles of $CaCO_3$ in the phase of vaterita for application in TFD [38]. The authors demonstrated a significant phototoxic effect using the MTT assay. A drastic difference was observed in the percentage of viable cells: 2% *versus* 20 %, for the encapsulated and free photosensitizer, respectively.

Wang et al. (2018) describe the synthesis of calcium carbonate-doxorubicin@silica-indocyanine green nanospheres for combined thermal, chemo and photodynamic therapeutic effects against drug-

resistant breast cancer cells [39]. The authors show that nanoparticulate sytem effectively induces cell death *via* photothermal effects and, a much lower cell viability of 12 % was observed for samples.

Confocal laser scanning microscopy was used to examine the internalization of ClAlPc-loaded $CaCO_3$ microparticles. It is possible to observe the internalization of phthalocyanine after one hour of incubation, at 37 °C, with the PS distributed in the cytoplasm, in both concentrations tested. The phthalocyanine concentration in the region corresponding to the nucleus is also observed, overlapping the signal with the nuclear material (arrow). The photosensitizer loaded in $CaCO_3$ microparticles predominated in nuclear and perinuclear regions. The results from confocal microscopy strongly indicate that ClAlPc-loaded $CaCO_3$ microparticles were uptaken by murine RAW 264.7 cell line. Vivero-Escoto et al. (2015) showed that the mesoporous silica nanoparticles-loaded with aluminum chloride phthalocyanine can be readily internalized in HeLa cells [40]. Xing et al. describe the fabrication of doxorubicin hydrochloric acid-loaded mesoporous $CaCO_3$ nanoparticles as intelligent carrier. The authors suggest the efficient cellular uptake of the nanoparticles that concentrated rapidly in the nuclei region in HeLa cells [41].

5. Conclusion

Vaterite microparticles are synthesized by a PSS-assisted precipitation route. The system proposed as drug delivery system was successfully manufactured, which was proven by the characterizations of XRD, SEM and BET, with particles in the micrometric scale, spherical morphology and with consequent apparent porosity. These factors made it possible to incorporate the drug without altering its physical-chemical properties, such as absorption in the Uv–vis region. IR spectroscopy indicated that the adsorption of the ClAlPc photosensitizer on the $CaCO_3$ microparticles is of a physical nature, which was corroborated by the XRD result. The phthalocyanine internalization process showed the PS distributed in the cytoplasm, in both concentrations tested, and the presence of ClAlPc in a region corresponding to the nucleus, overlapping the signal with the nuclear material. By the cell viability by trypan blue exclusion method it was possible to observe a significant reduction in viability in the groups treated with the highest concentration, of 3 $\mu mol.L^{-1}$, reaching approximately 80 % reduction in the group treated with 10 $J.cm^{-2}$. This factor can be attributed to the maximization of the photosensitizer properties when encapsulated in a release system for bioactive compounds. Summation of these effects with the simplicity, scalability and low cost of manufacture, biocompatibility and high carrying capacity of the particles of vaterita presents the potential use of calcium carbonate particles for photodynamic therapy and photoprocesses.

Acknowledgments

The authors acknowledge the financial support of the Brazilian agency FAPESP (Fundação de Amparo à Pesquisa do Estado de São Paulo) with project numbers 2018/18531-6.

References

[1] A.T.P.C. Gomes, M.G.P.M.S. Neves, J.A.S. Cavaleiro, Cancer, photodynamic therapy and porphyrin-type derivatives, An Acad Bras Ciênc (2018) 993–1026.
[2] P. Jia, C. Dai, P. Cao, D. Sun, R. Ouyang, et al., The role of reactive oxygen species in tumor treatment, RSC Adv. (2020) 7740–7750.
[3] X. Shi, C.Y. Zhang, J. Gao, Z. Wang, Recent advances in photodynamic therapy for cancer and infectious diseases, Wiley Interdiscip. Rev. Nanomed. Nanobiotechnol. (2019) e1560.
[4] M. Gallardo-Villagrán, D.Y. Leger, B. Liagre, B. Therrien, Photosensitizers used in the photodynamic therapy of rheumatoid arthritis, Int. J. Mol. Sci. (2019) 3339–3359.
[5] L. Li, K.M. Huh, Polymeric nanocarrier systems for photodynamic therapy, Biomater. Res. (2014) 19–32.
[6] S. Sansaloni-Pastor, J. Bouilloux, N. Lange, The Dark Side: Photosensitizer Prodrugs, Pharmaceuticals, 2019, pp. 148–166.
[7] M. Ethirajan, Y. Chen, P. Joshi, R.K. Pandey, The role of porphyrin chemistry in tumor imaging and photodynamic therapy, Chem. Soc. Rev. (2011) 340–362.
[8] J. Kou, D. Dou, L. Yang, Porphyrin photosensitizers in photodynamic therapy and its applications, Oncotarget (2017) 81591–81603.
[9] M. Lan, S. Zhao, W. Liu, C.S. Lee, W. Zhang, et al., Photosensitizers for photodynamic therapy, Adv. Healthc. Mater. (2019) e1900132.
[10] N. Mehraban, H.S. Freeman, Developments in PDT sensitizers for increased selectivity and singlet oxygen production, Materials (Basel) (2015) 4421–4456.
[11] C.M. Allen, W.M. Sharman, J.E.V. Lier, Current status of phthalocyanines in the photodynamic therapy of cancer, J. Porphyr. Phthalocya (2011) 161–169.
[12] E. Paszko, C. Ehrhardt, M.O. Senge, D.P. Kelleher, J.V. Reynolds, Nanodrug applications in photodynamic therapy, Photodiagn. Photodyn. Ther. (2011) 14–29.
[13] J. Rak, P. Pouckova, J. Benes, D. Vetvicka, Drug delivery systems for phthalocyanines for photodynamic therapy, Anticancer Res. (2019) 3323–3339.
[14] G.M.F. Calixto, J. Bernegossi, L.M. de Freitas, C.R. Fontana, M. Chorilli, Nanotechnology-based drug delivery systems for photodynamic therapy of cancer: a review, Molecules (2016) 342–359.
[15] S.M. Dizaj, M. Barzegar-Jalali, M.H. Zarrintan, K. Adibkia, F. Lotfipour, Calcium carbonate nanoparticles as cancer drug delivery system, Expert Opin. (2015) 1744–7593.
[16] L.M.M. Costa, G.M. Olyveira, R. Salomão, Precipitated calcium carbonate nano-microparticles: applications in drug delivery, Adv. Tissue Eng. Regen. Med. Open Access (2017) 336–340.
[17] A. Sarkar, S. Mahapatra, Synthesis of all crystalline phases of anhydrous calcium carbonate, Cryst. Growth Des. (2010) 2129–2135.
[18] A. Declet, E. Reyes, O.M. Suarez, Calcium carbonate precipitation: a review of the carbonate crystallization process and applications in bioinspired composites, Rev Adv. Mater. Sci. (2016) 87–107.
[19] D. Konopacka-Łyskawa, Synthesis methods and favorable conditions for spherical vaterite precipitation: a review, Crystals (2019) 223–238.
[20] M. Ghiasi, M. Abdollahy, M.R. Khalesi, E. Ghiasi, Control of the morphology, specific surface area and agglomeration of precipitated calcium carbonate crystals through a multiphase carbonation process, CrystEngComm (2020) 1970–1984.
[21] L. Kabalah-Amitai, B. Mayzel, Y. Kauffmann, A.N. Fitch, L. Bloch, et al., Vaterite crystals contain two interspersed crystal structures, Science (2013) 457-457.
[22] O. Gusliakova, E.N. Atochina-Vasserman, O. Sindeeva, S. Sindeev, S. Pinyaev, et al., Use of submicron vaterite particles serves as an effective delivery vehicle to the respiratory portion of the lung, Front. Pharmacol. (2018) 559–571.
[23] A. Vikulina, D. Voronin, R. Fakhrullin, V. Vinokurov, D. Volodkin, Naturally derived nano- and micro-drug delivery vehicles: halloysite, vaterite and nanocellulose, New J. Chem. (2020) 5638–5655.
[24] M.E.S.I. Saraya, H.H.A.L. Rokbaa, Preparation of vaterite calcium carbonate in the form of spherical nano-size particles with the aid of polycarboxylate superplasticizer as a capping agent, Am. J. Nanomater. (2016) 44–51.
[25] Y. Boyjoo, V.K. Pareek, J. Liu, Synthesis of micro and nano-sized calcium carbonate particles and their applications, J. Mater. Chem. (2014) 14270–14288.
[26] J. Song, R. Wang, Z. Liu, H. Zhang, Preparation and characterization of calcium carbonate microspheres and their potential application as drug carriers, Mol. Med. Rep. (2018) 8403–8408.
[27] F.C. Donnelly, F. Purcell-Milton, V. Framont, O. Cleary, P.W. Dunne, et al., Synthesis of CaCO3 nano- and micro-particles by dry ice carbonation, Chem. Commun. (2017) 6657–6660.
[28] D.B. Trushina, T.V. Bukreeva, M.N. Antipina, Size-controlled synthesis of vaterite calcium carbonate by the mixing method: aiming for nanosized particles, Cryst. Growth Des. (2016) 1311–1319.
[29] S.E. Facchinetto, T. Bortolotto, G.E. Neumann, J.C.B. Vieira, B.B. de Menezes, et al., Synthesis of submicrometer calcium carbonate particles from inorganic salts using linear polymers as crystallization modifiers, J. Braz. Chem. Soc. (2017) 547–556.
[30] K. Naka, Y. Chujo, Control of crystal nucleation and growth of calcium carbonate by synthetic substrates, Chem. Mater. (2001) 3245–3259.
[31] T. Beuvier, B. Calvignac, G.J.R. Delcroix, M.K. Tran, S. Kodjikian, et al., Synthesis of hollow vaterite CaCO3 microspheres in supercritical carbon dioxide medium, J. Mater. Chem. (2011) 9757–9761.
[32] G.B. Sukhorukov, D.V. Volodkin, A.M. Gunther, A.I. Petrov, D.B. Shenoy, et al., Porous calcium carbonate microparticles as templates for encapsulation of bioactive compounds, J. Mater. Chem. (2004) 2073–2081.
[33] A.I. Petrov, D.V. Volodkin, G.B. Sukhorukov, Protein-calcium carbonate coprecipitation: a tool for protein encapsulation, Biotechnol. Prog. (2005) 918–925.
[34] K.G.M.D. Abeykoon, S.P. Dunuweera, D.N.D. Liyanage, R.M.G. Rajapakse, Removal of fluoride from aqueous solution by porous Vaterite calcium carbonate nanoparticles, Mater. Res. Express (2020) 035009–0350020.
[35] C. Wang, C. He, Z. Tong, X. Liu, B. Ren, F. Zeng, Combination of adsorption by porous CaCO3 microparticles and encapsulation by polyelectrolyte multilayer films for sustained drug delivery, Int. J. Pharm. (2006) 160–167.
[36] H. Benachour, A. Sève, T. Bastogne, C. Frochot, R. Vanderesse, et al., Multifunctional Peptide-conjugated hybrid silica nanoparticles for photodynamic therapy and MRI, Theranostics (2012) 889–904.
[37] S.Ç. Uzuner, Development of a direct trypan blue exclusion method to detect cell viability of adherent cells into ELISA plates, CBU J. Sci. (2018) 99–104.
[38] Y.I. Svenskaya, A.M. Pavlov, D.A. Gorina, D.J. Gould, B.V. Parakhonskiy, Photodynamic therapy platform based on localized delivery of photosensitizer by vaterite submicron particles, Colloids Surf. B Biointerfaces (2016) 171–179.
[39] W. Wang, Y. Zhao, B.B. Yan, L. Dong, Y. Lu, S.H. Yu, Calcium carbonate-doxorubicin@silica-indocyanine green nanospheres with photo-triggered drug delivery enhance cell killing in drug-resistant breast cancer cells, Nano Res. (2018) 3385–3395.
[40] J.L. Vivero-Escoto, M. Elnagheeb, Mesoporous silica nanoparticles loaded with cisplatin and phthalocyanine for combination chemotherapy and photodynamic therapy in vitro, Nanomaterials (2015) 2302–2316.
[41] J. Xing, Y. Cai, Y. Wang, H. Zheng, Y. Liu, Synthesis of polymer assembled mesoporous CaCO3 nanoparticles for molecular targeting and pH-Responsive controlled drug release, Adv. Polym. Technol. (2020) 8749238–8749245.